Stopping power of some lightly ionized gold ions for protons

E. J. McGuire
Sandia National Laboratories, Albuquerque, New Mexico 87185
(Received 23 March 1981; revised manuscript received 19 April 1982)

Calculations are presented for the stopping power of Au^{n+} $(0 \leq n \leq 11)$ for protons with energy between 0.1 and 10 MeV. Over this range the proton stopping power changes by at least a factor of 2 between neutral and 11 times ionized gold. Explicit Born-approximation calculations are done for both excitation (for all ions considered) and ionization (for selected ions). For inner shells ($nl \leq 4d$) the explicit calculations are in excellent agreement with results obtained from scaling laws. For outer shells ($nl \geq 4f$) there are differences of as much as a factor of 2 between the explicit calculations and the scaling laws for some subshells of some ions. A correction to the scaling laws using an integral over optical oscillator strength is developed which removes some of the disagreement between the explicit calculations and scaled values. The residual difference between the explicit calculations and the scaled values appears to arise from the spatial expansion of an ion subshell orbital compared to an atom subshell orbital even when the subshells have the same ionization energy.

I. INTRODUCTION

In the preceding paper[1] I described a program for calculating proton stopping power in ions and atoms by explicitly determining subshell excitation and ionization generalized oscillator strengths (GOS), integrating over the GOS to determine subshell contributions to the stopping power, and summing the subshell contributions to determine the total stopping power. Of necessity, the sum is truncated; the excitation calculations are limited to a finite number (10—15) of excited levels and a finite (2—4) number of outer occupied levels; scaling laws are used for inner-shell ionization; and a δ function is used to approximate the high-energy region of the GOS not included in the explicit GOS calculations. The agreement with experimental measurements on neutral atoms (15% or better) indicates the error arising from both the truncation used and the use of the plane-wave Born approximation (PWBA). For neutral atoms one expects the PWBA to be reasonably accurate for proton energies (E_p) greater than $(M_p/M_e)E_{nl}$, where E_{nl} is the subshell ionization energy. At lower energies the PWBA becomes less accurate as E_p decreases, but for such energies the ionization cross section and contribution to stopping power falls rapidly with decreasing E_p. Thus, one does not expect the use of the PWBA to introduce significant error in the neutral atom stopping-power calculations for proton energies above 0.1 MeV.

Thus, the comparisons with experiment in the preceding paper check the adequacy of the truncation procedures rather than the adequacy of the PWBA. Here the PWBA is being used to calculate the proton stopping power of ions. While it is well known that the PWBA predicts zero excitation cross sections near threshold for ions, whereas the cross sections are actually finite, other than near threshold the PWBA is in remarkable agreement[2] with experiment (20%) and Coulomb-Born calculations (15%) for electron-ion ionization calculations in low-Z ions. It is assumed that this agreement will persist for high-Z ions, and to verify this assumption PWBA calculations will be performed as the high-Z experiments become available. Further, inner shells contribute significantly to stopping power, and if the inner shells are treated accurately by the PWBA for neutral atoms there is no inherent reason not to assume a PWBA treatment is accurate for inner shells of ions.

As discussed in Sec. VII of the preceding paper, while it is traditional to discuss stopping power in the framework of the Bethe theory[3] $[(-1/n)dE/dx] \propto [\ln(4M_eE_p/M_pI)+\cdots]$ where the ellipsis stands for corrections, this format is not followed here. The proton energy range of interest here is low, the corrections are likely to be large, and all subshells contribute to the corrections including those that contribute negligibly to the stopping power. The traditional framework imposes the foolish requirement that one calculate GOS for sub-

shells that are irrelevant to the stopping power. When explicit GOS calculations are done for the ions herein, they are done for subshells that do contribute significantly to the stopping power for proton energies below 10 MeV.

In practice the ions treated here exist in a plasma and there are additional energy-loss mechanisms arising from the plasma, e.g., collective energy losses to the plasma electrons. These are discussed by Mehlhorn,[4] and are not further treated here.

In the preceding paper scaling laws for the subshell ionization contribution to stopping power were obtained. For neutral atoms the scaling laws are essentially interpolation formulas. In the comparisons with experiment in Ref. 1 the scaling laws for ionization were used in place of explicit calculations. One purpose of this paper is to assess the validity of extrapolating the scaling laws to ions by comparison with explicit calculations on gold ions. No scaling laws for the excitation contribution to subshell stopping power have been found and these calculations are done explicitly. For this study of gold ions, excitation calculations are done with occupied $4f$, $5s$, $5p$, and $5d$ subshells, and empty or partially filled $6s$-$8s$, $6p$-$8p$, $5d$-$8d$, $5f$, $6f$, and $5g$ subshells. In general, the outer subshells and, in particular, the resonance transitions (e.g., $5p$-$5d$) dominate the excitation contribution to stopping power. In Ref. 3 it was pointed out that this was also true in the transition elements where the $(3p)^6(3d)^n$-$(3p)^5(3d)^{n+1}$ transition dominated the contribution of excitation to stopping power.

In Sec. II the results for the calculated proton stopping power are presented. As electrons are stripped away the contribution of ionization to stopping power is reduced both because outer electrons are removed and ionization energies are increased. The contribution of excitation to stopping power initially increases in absolute value because a resonance transition previously forbidden by the Pauli principle becomes allowed (here the $5p$-$5d$ transition). However, with increasing ionization the absolute value of the excitation contribution to stopping power decreases because the excitation cross section drops off rapidly with increasing resonance transition energy. This picture was earlier suggested by Hahn[5]; the results in Sec. II quantify it. The surprising feature of the results in Sec. II is the large (factor of 2 or larger) change in stopping power with a small degree of ionization.

While the scaling laws for the contribution of subshell ionization to stopping power do a satisfactory job when summed over subshells, when compared with explicit calculations, they are in error by as much as a factor of 2 at high energy. In Sec. III comparison is made of the explicit calculations and scaling-law results for subshell ionization stopping power. Comparison is also made of the calculated ionic generalized oscillator strength (GOS) and the calculated GOS for atoms of comparable ionization energy for the $4f$ and $5d$ subshells. Agreement of these two calculations for a given subshell is a sufficient condition for the validity of the scaling laws. It is found that the disagreement between the two calculations occurs at small momentum transfers, i.e., large-distance collisions. This suggests a correction to the scaling hypothesis involving the $K^2=0$ GOS, the optical oscillator strength, and this is investigated in Sec. IV. The conclusions are in Sec. V.

II. THE STOPPING POWER

The explicit calculations approximate $-rV(r)$ of Herman and Skillman[6] for the ions with a series of nine straight lines.[7] Because the gold-ion potentials become more compact with the degree of ionization, the approximation with nine straight lines becomes increasingly more accurate and in the calculations the difference between model and Herman-Skillman eigenvalues is never more than 3%. With the model potential, eigenvalues are calculated for both occupied and unoccupied levels. These eigenvalues and eigenfunctions are used to calculate excitation GOS as described in the preceding paper.[3]

The calculated excitation stopping power for gold ions is shown in Fig. 1 for protons from 0.1 to 10 MeV. The excitation stopping power decreases at low energy in going from neutral to singly ionized gold due to the removal of the $6s$ electron. With further ionization the excitation stopping power in-

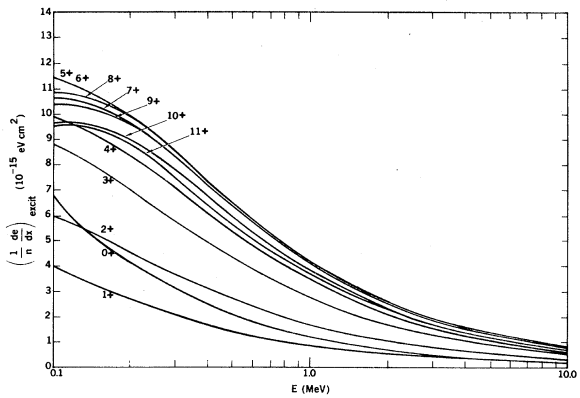

FIG. 1. The calculated stopping power of gold ions due to excitation.

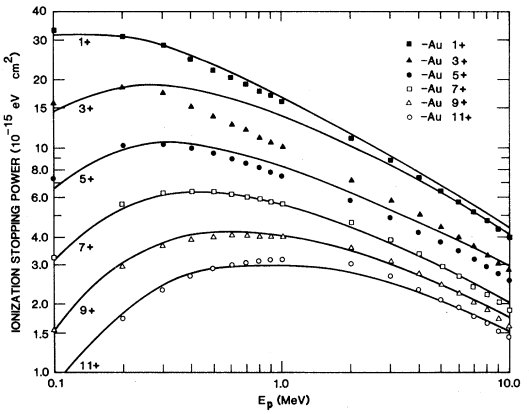

FIG. 2. Comparison of the contribution to the stopping power of gold ions due to ionization of the $4f+5s+5p+5d+6s$ subshells. The solid lines are scaled stopping-power results and the points are explicit calculations. Both calculations include a Bethe-ridge correction.

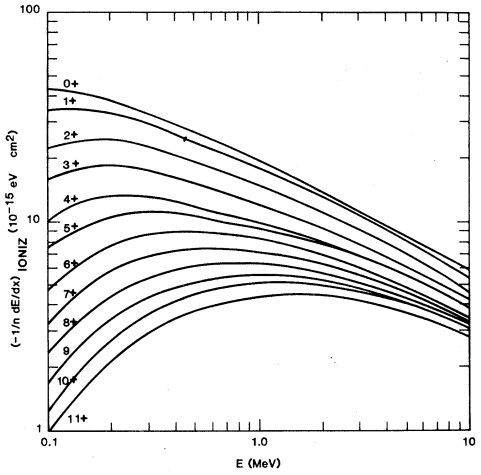

FIG. 3. The calculated stopping power of gold ions due to ionization.

creases as the $(5p)^6(5d)^n \rightarrow (5p)^5(5d)^{n+1}$ transition becomes dominant, peaks with the $5d$ subshell half filled, then decreases slowly. To illustrate this behavior (and to show the difficulty in separating the curves in Fig. 1) Table II lists the contribution to stopping power of excitation of the outermost four subshells at 1 MeV as a function of degree of ionization.

To save computer time in calculating the GOS for ionization, initially only Au^{0+} and Au^{n+} with n odd were treated. The subshells included were $4p$-$6s$. As shown in Sec. III the explicit calculations and scaling laws are in excellent agreement for the $4p$ and $4d$ subshells. In Fig. 2 the summed contribution of the $4f$, $5s$, $5p$, and $5d$ subshells are shown. The solid lines are the scaled results, the points are explicit calculation. The correction[1] for the neglected Bethe ridge[4] is an integral part of the scaled stopping-power computer routine. The Bethe-ridge correction was added to the values calculated explicitly. For Au^{7+}, Au^{9+}, and Au^{11+}, the scaled and explicit calculations are in excellent agreement. For Au^{1+} they differ by no more than 10%. For Au^{5+} the difference is as much as 20%; however, when inner shell ($nl \leq 4d$) ionization and outer-shell excitation are added this difference is less than 10% of the total stopping power. For Au^{3+} there is a substantial disagreement. As a result, explicit calculations were done for the $4f$, $5s$, $5p$, and $5d$ subshells of Au^{2+} and Au^{4+}. In Fig. 3 the total ionization contribution to stopping power is shown for Au^{n+}. For $n=0$ and $n \geq 6$ scaled values were summed; for $1 \leq n \leq 5$ scaled values were used for inner subshells $nl \leq 4d$, and explicit calculations for outer subshells $nl \geq 4f$.

Total (excitation plus ionization) stopping powers are listed in Table II. In comparing neutral and 11 times ionized gold one finds the stopping power is reduced by factors 0.385, 0.516, and 0.578 at 1.0, 4.0, and 10.0 MeV, respectively. Between 3 and 10 MeV the calculated stopping power of Au^{5+} is greater than that of Au^{4+}. This arises from the enhanced excitation stopping power calculated for Au^{5+}. However, the difference in stopping power in the two cases is less than 5% and may be a numerical artifact.

While it is probably dubious to invoke a Bethe formula[4] (without inner-shell corrections) for these ions, in this range of proton energies, the formula

TABLE I. The excitation contribution to stopping power (10^{-15} eV cm^2) of the outer four subshells at 1 MeV as a function of degree of ionization.

nl \ Z	+5	+6	+7	+8	+9	+10
$4f$	0.18	0.22	0.28	0.31	0.35	0.42
$5s$	0.17	0.20	0.23	0.27	0.30	0.31
$5p$	1.40	1.65	1.87	2.14	2.45	2.65
$5d$	2.40	2.20	1.70	1.45	1.05	0.485
Total	4.15	4.27	4.08	4.17	4.15	3.87

TABLE II. The calculated stopping power of Au^{n+} ($0 \leq n \leq 11$) for protons with 0.1 MeV $\leq E_p \leq 10$ MeV. The I/Z values are obtained from the calculations at 10 MeV and a Bethe formula without inner-shell corrections.

	Stopping power (10^{-15} eV cm^2)											
E_p (MeV) \ Au^{n+}	0	1	2	3	4	5	6	7	8	9	10	11
0.1	49.7	37.9	28.7	24.7	19.8	18.9	16.1	14.0	13.1	12.1	10.9	10.5
0.2	41.8	35.7	29.3	25.5	21.5	20.7	17.7	15.4	14.4	13.0	11.7	10.9
0.3	35.6	31.4	26.6	23.4	20.1	19.6	17.2	15.0	13.9	12.6	11.4	10.4
0.4	31.6	27.8	24.1	21.1	18.6	18.2	16.3	14.4	13.3	12.0	10.8	9.86
0.5	28.3	25.5	22.0	19.2	17.3	17.1	15.5	13.7	12.8	11.5	10.4	9.20
0.6	26.5	23.5	20.4	18.1	16.0	16.0	14.7	13.1	12.1	10.9	9.97	9.01
0.7	24.4	22.2	19.3	17.0	15.2	15.3	14.1	12.6	11.8	10.6	9.60	8.55
0.8	23.1	20.9	18.2	16.0	14.3	14.6	13.5	12.1	11.2	10.2	9.33	8.42
0.9	21.6	19.8	17.4	15.3	13.7	14.0	13.0	11.7	10.9	9.90	9.15	8.15
1.0	20.7	18.8	16.7	14.7	13.2	13.5	12.5	11.2	10.5	9.56	8.85	7.97
2.0	14.5	13.8	12.1	10.9	10.0	10.3	9.58	8.81	8.30	7.68	7.34	6.63
3.0	11.7	11.2	9.80	9.10	8.40	8.65	8.01	7.44	7.06	6.60	6.41	5.80
4.0	10.1	9.34	8.50	7.80	7.31	7.54	6.96	6.50	6.20	5.84	5.75	5.21
5.0	8.80	8.45	7.42	6.98	6.58	6.82	6.20	5.78	5.60	5.23	5.15	4.75
6.0	8.03	7.62	6.58	6.35	5.97	6.19	5.68	5.32	5.10	4.83	4.81	4.36
7.0	7.30	6.95	6.10	5.80	5.52	5.67	5.15	4.90	4.72	4.43	4.40	4.05
8.0	6.83	6.38	5.62	5.37	5.11	5.29	4.86	4.61	4.43	4.21	4.19	3.82
9.0	6.30	5.90	5.20	5.00	4.78	4.93	4.45	4.28	4.13	3.92	3.90	3.60
10.0	5.93	5.51	4.84	4.68	4.46	4.64	4.27	4.07	3.92	3.74	3.74	3.43
I/Z (eV)	11.6	13.9	19.4	20.4	22.3	19.5	23.3	25.3	26.7	28.8	27.9	32.7

$$-\frac{1}{n}\frac{dE}{dX}=\frac{1.29\times10^{-16}(m_p/m_e)}{E_p\ (\text{keV})}Z_e\ln[4m_eE_p(\text{keV})/m_pI(\text{keV})]$$

can be used at 10 MeV to extract the I/Z values listed in Table II, where Z_e is the number of electrons on the ion and Z is the nuclear charge (79). For $2 \leq E_p \leq 10$ MeV, they will reproduce the calculated stopping power for Au^{0+} and Au^{1+} to better than 10%. For $4 \leq E_p \leq 10$ MeV, they will reproduce the calculated stopping power to better than 10% for Au^{n+} with $2 \leq n \leq 11$.

III. THE DISAGREEMENT BETWEEN SCALED AND EXPLICIT IONIC SUBSHELL STOPPING POWER

In Figs. 4–6 the calculated peak subshell stopping power due to ionization times subshell ionization energy is plotted versus subshell ionization energy for the $4p$ and $4d$, $4f$ and $5s$, and $5p$ and $5d$ subshells, respectively. For the $5d$ subshell, when necessary, calculations are adjusted to ten $5d$ electrons. The solid lines are neutral atom values while the open circles are for gold ions. For the $4p$ and $4d$ subshells there is excellent agreement between neutral atom and ion values; for the $4f$ and $5d$ subshells, the agreement is better than 25%, while for the $5s$ and $5p$ subshells, the disagreement for Au^{11+} is between 30% and 50%. These plots were used in Ref. 1 to obtain the scaled subshell stopping powers

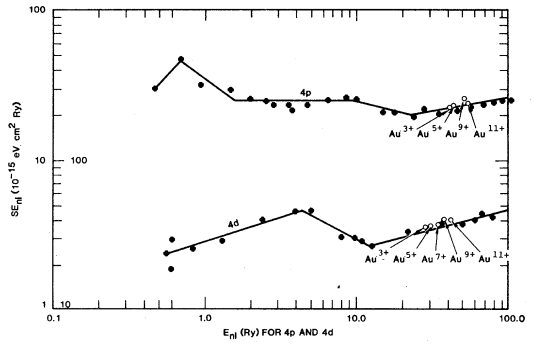

FIG. 4. Peak subshell ionization stopping power times subshell ionization energy versus subshell ionization energy for the $4p$ and $4d$ subshells. The crosses and solid lines are neutral-atom calculations. The labeled open circles are calculated for gold ions.

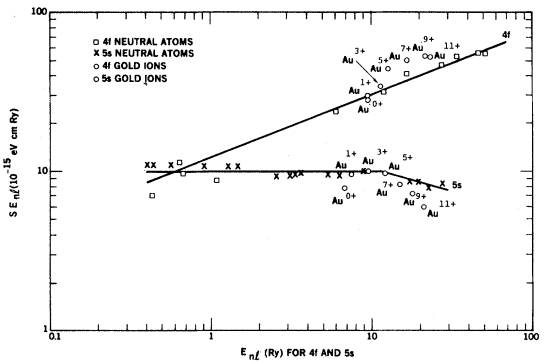

FIG. 5. Peak subshell ionization stopping power times subshell ionization energy versus subshell ionization energy for the $4f$ and $5s$ subshells. The solid lines are neutral-atom calculations. The labeled open circles are calculated for gold ions.

from neutral-atom calculations. As will be shown, these plots underestimate the departure of the explicit calculations from the scaling laws for outer subshells.

In Fig. 7 the scaled subshell stopping powers for Au^{3+} subshells are shown as solid lines, and the explicitly calculated values including the Bethe-ridge correction are shown as points. The dashed lines are corrections to the scaling laws as discussed in Sec. IV. For the $4p$, $4d$, $4f$, and $5s$ subshells, there is good agreement between the two sets of calculations. For the $5p$ and $5d$ subshells there is significant disagreement, 30% for the $5p$, and 100% for the $5d$ at 10 MeV. In Fig. 8 similar calculations are

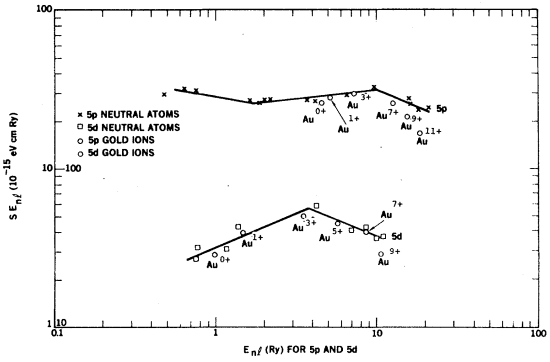

FIG. 6. Peak subshell ionization stopping power times subshell ionization energy versus subshell ionization energy for the $5p$ and $5d$ (normalized to ten electrons) subshells. The solid lines are neutral-atom calculations. The labeled open circles are calculated for gold ions.

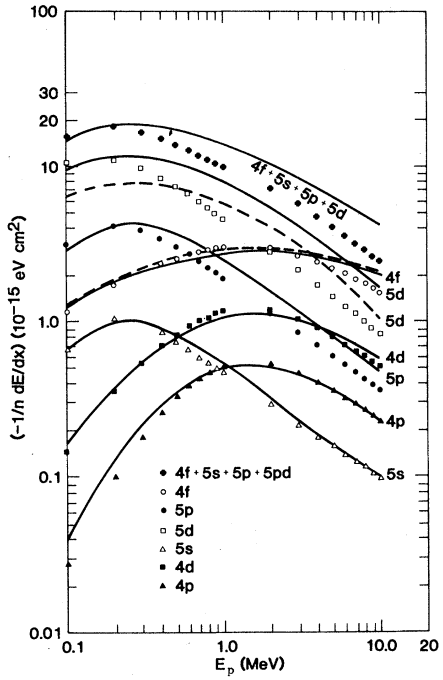

FIG. 7. Proton energy dependence of subshell ionization stopping power for Au^{3+}. The solid curves are scaling-law values. The points are explicit calculations. The dashed lines are corrected scaling-law values for the $4f$ and $5d$ subshells.

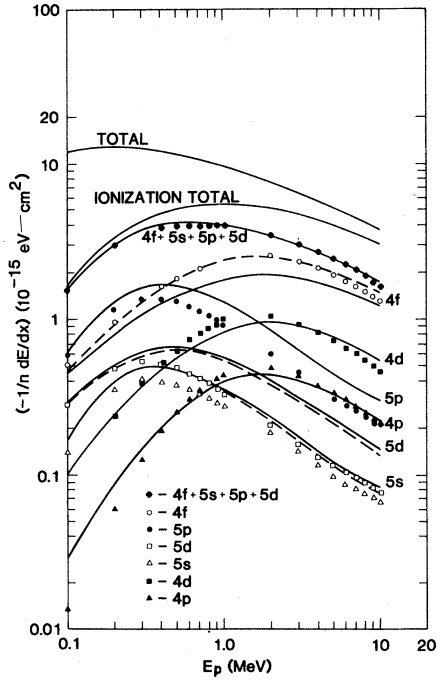

FIG. 8. Proton energy dependence of subshell ionization stopping power for Au^{9+}. The solid curves are scaling-law values. The points are explicit evaluations. The dashed lines are corrected scaling-law values for the $4f$, $5s$, and $5d$ subshells.

shown for Au^{9+}. The scaled values are shown as solid lines and the explicit calculations, including the Bethe-ridge correction, are shown as points. Here for the $4p$ and $4d$ subshells there is good agreement between the two sets of calculations, which is why, in Sec. II, we used scaled stopping powers for all subshells with $nl \leq 4d$. For the $4f$ subshell the explicit calculations are larger, and for the $5s$, $5p$, and $5d$ subshells, smaller than the scaled values. The differences cancel when the stopping power is summed over subshells, leading to the good agreement between the two sets of calculations in Fig. 2 for $n \geq 7$. An interesting feature of the explicit calculations in Fig. 8 is that in the MeV regime, the contributions of the $5s$ and $5d$ subshells, both with two electrons, are almost equal, while the contribution of the $5p$ subshell with six electrons is three times that of either the $5s$ or $5d$ subshell, and above 2 MeV almost equal to the contribution of the $4p$ subshell. That is, for these outer subshells, the ionization stopping power is independent of the subshell ionization energy and one can treat all 16 electrons as equivalent in stopping. Note that this equivalence is not seen for Au^{3+} in Fig. 7.

Figures 7 and 8 indicate that for ions the scaling laws for subshells can be inaccurate at high energy by as much as a factor of 2. Differences of as much as a factor of 2 were found[8] in comparing measured electron ionization cross sections for low-Z ions with cross sections obtained from scaled electron ionization cross sections.

To improve the accuracy of the scaling laws one must examine the cause of their breakdown; i.e., how does the subshell generalized oscillator strength change in going from a neutral atom to an ion when both subshells have comparable ionization energy. In Fig. 9 such a comparison is made for the $5d$ subshell of Rn($Z=86$), with model ionization energy of 4.16 Ry, and the $5d$ subshell of Au^{3+} (adjusted to ten electrons) with model ionization energy of 3.49 Ry. A wide range of both K^2/E_{5d} and E/E_{5d} is described in Fig. 9 (note the break in the $(K^2/E_{5d})^{1/2}$ scale). For $K^2/E_{5d} > 1$ there is reasonable agreement between the neutral-atom GOS (solid lines) and Au^{3+} GOS (points). For $(K^2/E_{5d})^{1/2} < 1$ there is moderate agreement at $\epsilon/E_{5d}=1.0$ and 10.0, but differences of a factor of 2 or more at $\epsilon/E_{5d}=0.001$, 0.1, and 25. To the extent that the high-energy subshell ionization stopping power is dominated by small K^2/E_{5d} values (near the optical limit of the GOS) and small ϵ/E_{5d} values, the upper-left-hand corner of Fig. 9 can account for the factor of 2 difference in the $5d$ cross section shown in Fig. 7. As pointed out in the

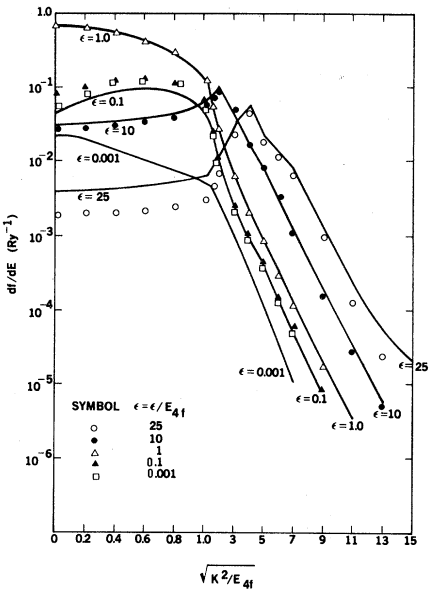

FIG. 9. Calculated GOS for the $5d$ subshell of Rn with $Z=86$ and $E_{5d}=4.16$ Ry (solid lines) and Au^{3+} with $E_{5d}=3.49$ Ry (points) for $\epsilon/E_{5d}=0.001$, 0.1, 1.0, 10.0, and 25.0. There is a change of abscissa scale at $K^2/E_{5p}=1$.

preceding paper,[1] one-electron calculations on the $5d$ photoionization cross section of neutral atoms near $Z=86$ show a remarkable resonancelike structure,[9] but the variation in the resonancelike struc-

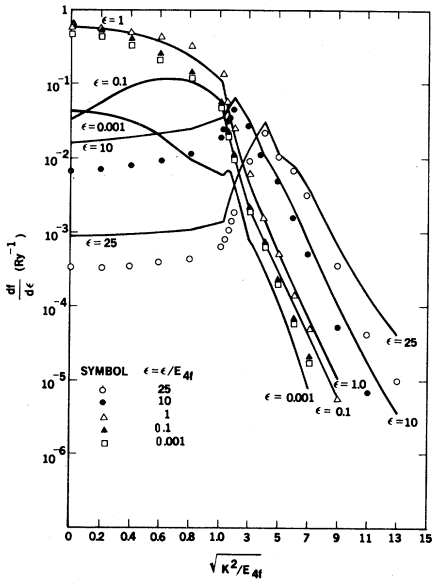

FIG. 10. Calculated GOS for the $4f$ subshell of Pb with $Z=82$ and $E_{4f}=11.87$ Ry (solid lines) and Au^{3+} with $E_{4f}=11.39$ Ry (points) for $\epsilon/E_{4f}=0.001$, 0.1, 1.0, 10.0, and 25.0. There is a change of abscissa scale at $K^2/E_{4f}=1$.

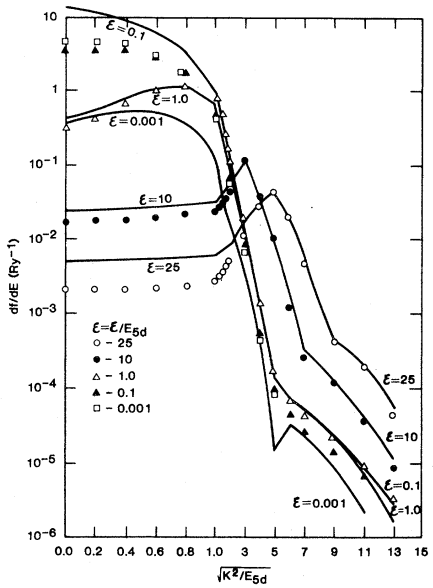

FIG. 11. Calculated GOS for the $4f$ subshell of Rn with $Z=86$ and $E_{4f}=16.67$ Ry (solid lines) and Au^{7+} with $E_{4f}=16.59$ (points) for $\epsilon/E_{4f}=0.001$, 0.1, 1.0, 10.0, and 25.0. There is a change of abscissa scale at $K^2/E_{4f}=1$.

ture with Z did not distort the scaled subshell stopping power in neutral atoms. For the ion it does.

A GOS comparison with comparable results (i.e., significant differences at $K^2/E_n<1$) is found for the $5s$ and $5p$ subshells. The $4f$ subshell shows different results. In Fig. 10 the $4f$ GOS for $Z=82$ ($E_{4f}=11.87$ Ry) is compared with calculations for Au^{3+} ($E_{4f}=11.39$ Ry), while Fig. 11 shows a comparison for $Z=86$ ($E_{4f}=16.60$ Ry) and Au^{7+} ($E_{4f}=16.59$ Ry). In Fig. 10 there is good agreement between the two sets of GOS except for $\epsilon/E_{4f}=0.001$ and 25 at $K^2/E_{4f}<1$. As Fig. 7 showed for Au^{3+}, the scaled and explicitly calculated $4f$ stopping power were in excellent agreement. Figure 8, for Au^{9+}, showed that the explicit calculation of $4f$ stopping power was larger than the scaled values. The upper-left-hand corner of Fig. 11 shows that for $E_{4f}=0.001$ and 0.1 the Au^{7+} GOS is considerably larger than the neutral-atom values at $Z=86$.

In Sec. IV these intercomparisons of GOS are used to construct a correction to the scaling hypothesis for ions.

IV. CORRECTIONS TO THE SUBSHELL SCALING LAWS

The subshell ionization cross section or stopping power for incident protons or electrons can be written[4]

$$S(E,q)=\frac{4\pi a_0^2}{m_e E/m}\int_0^{E_u}\frac{d\epsilon}{(\epsilon+E_{nl})^q}\int_{K^2_{\min}}^{K^2_{\max}}\frac{dK^2}{K^2}\frac{df_{nl}}{d\epsilon}(\epsilon,K^2)\ , \tag{1}$$

where E and m are the projectile energy and mass, and E_u is E_p-E_{nl} for protons and $\frac{1}{2}(E_e-E^z_{nl})$ for electrons. The momentum transfer limits are given by

$$(K^2)^{\max}_{\min}=\frac{m}{m_e}(\sqrt{E}\pm\sqrt{E-\epsilon-E_{nl}})^2\ . \tag{2}$$

The parameter q is zero for stopping-power calculations and unity for ionization calculations. Consider the nl subshell of an ion with ionization energy E^z_{nl}, nuclear charge Z, and net charge z, the nl subshell of a pseudoatom with ionization energy E^z_{nl}, nuclear charge Z', and net charge zero, and a neutral atom with subshell ionization energy E^0_{nl}, nuclear charge Z, and net charge zero. The generalized oscillator strength is written

$$\frac{df_{nl}}{d\epsilon}(\epsilon,K^2,E_{nl},Z,z)$$

and without loss of generality we may write

$$\frac{df_{nl}}{d\epsilon}(\epsilon,K^2,E^Z_{nl},Z,z)=\Theta(K^2/E^Z_{nl}-1)\frac{df^L_{nl}}{d\epsilon}(\epsilon,K^2,E^Z_{nl},Z,z)+\Theta(1-K^2/E^Z_{nl})\frac{df^S_{nl}}{d\epsilon}(\epsilon,K^2,E^Z_{nl},Z,z)\ , \tag{3}$$

where S and L indicate small and large K^2/E_{nl}. Then providing $E_u>\epsilon_1$ where

$$\epsilon_1=\left[\frac{4m_eE}{m}E^Z_{nl}\right]^{1/2}-\left[1+\frac{m_e}{m}\right]E^Z_{nl}\ .$$

We have

$$S(E,E_{nl}^Z,Z,z)=\frac{4\pi a_0^2}{(m_eE/m)}\left[\int_0^{\epsilon_1}\frac{d\epsilon}{(\epsilon+E_{nl}^Z)^q}\int_{K_{\min}^2}^{E_{nl}^Z}\frac{dK^2}{K^2}\frac{df_{nl}^S}{d\epsilon}(\epsilon,K^2,E_{nl}^Z,Z,z)\right.$$
$$\left.+\int_0^{E_u}\frac{d\epsilon}{(\epsilon+E_{nl}^Z)^q}\int_{E_{nl}^Z}^{K_{\max}^2}\frac{dK^2}{K^2}\frac{df_{nl}^L}{d\epsilon}(\epsilon,K^2,E_{nl}^Z,Z,z)\right]. \quad (4)$$

The intercomparison of generalized oscillator strengths in Figs. 9—11 suggests that it is a reasonable approximation to use

$$\frac{df_{nl}^L}{d\epsilon}(\epsilon,K^2,E_{nl}^Z,Z,z)=\frac{df_{nl}^L}{d\epsilon}(\epsilon,K^2,E_{nl}^Z,Z',0)\ ;$$

i.e., for $K^2/E_{nl}^Z>1$, the neutral-atom and ion GOS are equal if the ionization energies are equal. Then adding and subtracting

$$\frac{4\pi a_0^2}{m_eE/m}\int_0^{E_1}\frac{d\epsilon}{(\epsilon+E_{nl}^Z)^q}\int_{K_{\min}^2}^{E_{nl}^Z}\frac{dK^2}{K^2}\frac{df_{nl}^S}{d\epsilon}(\epsilon,K^2,E_{nl}^Z,Z',0)$$

leads to the scaling result with a correction term, i.e.,

$$S(E,E_{nl}^Z,Z,z)=S(E,E_{nl}^Z,Z',0)$$
$$+\frac{4\pi a_0^2}{(m_eE/m)}\int_0^{\epsilon_1}\frac{d\epsilon}{(\epsilon+E_{nl})^q}\int_{K_{\min}^2}^{E_{nl}^Z}\frac{dK^2}{K^2}\left[\frac{df_{nl}^2}{d\epsilon}(\epsilon,K^2,E_{nl}^Z,Z,z)-\frac{df_{nl}^S}{d\epsilon}(\epsilon,K^2,E_{nl}^Z,Z',0)\right]. \quad (5)$$

The correction involves the GOS of both the ion and the pseudoatom, and the above development is not yet very useful. The correction term enters when $\epsilon_1>0$ or

$$E>\frac{m}{4m_e}E_{nl}^Z(1+m_e/m)^2\ . \quad (6)$$

For electrons this states $E>E_{nl}^Z$, an obvious condition, but for protons it requires $\eta=m_eE_p/m_pE_{nl}^Z>\frac{1}{4}$. There is a range of η where the correction does not enter. Further, for protons, from the definition of η and ϵ_1, one has

$$\epsilon_1/E_{nl}^Z=(4m_eE_p/mE_{nl}^Z)^{1/2}-1$$
$$=2\sqrt{\eta-1}\ . \quad (7)$$

For 10 MeV protons, with E_{nl}^Z in Ry, this becomes

$$\frac{\epsilon_1}{E_{nl}^Z}=\frac{40}{(E_{nl}^Z)^{1/2}-1}$$

and restricts the range of GOS contributing to the correction (e.g., for $E_{nl}^Z=16$ Ry, $\epsilon_1/E_{nl}^Z\leq 9$), i.e., the upper-left-hand regions of Figs. 9—11.

In Eq. (5) the integrand contains the difference of two GOS. If one assumes this difference is zero at $K^2=E_{nl}^Z$, and that it is linear in K^2 for $0\leq K^2\leq E_{nl}^Z$,

$$\left[\frac{df_{nl}^S}{d\epsilon}(\epsilon,K^2,E_{nl}^Z,Z,z)-\frac{df_{nl}^S}{d\epsilon}(\epsilon,K^2,E_{nl}^Z,Z',0)\right]=\frac{(E_{nl}^Z-K^2)}{E_{nl}^Z}\left[\frac{df_{nl}^S}{d\epsilon}(\epsilon,0,E_{nl}^Z,Z,z)-\frac{df_{nl}^S}{d\epsilon}(\epsilon,0,E_{nl}^Z,Z',0)\right] \quad (8)$$

and we have

$$S(E,E_{nl}^Z,Z,z)=S(E,E_{nl}^Z,Z',0)$$
$$+\frac{4\pi a_0^2}{(m_eE/m)}\int_0^{\epsilon_1}\frac{d\epsilon}{(\epsilon+E_{nl}^Z)^q}[\ln(E_{nl}^Z/K_{\min}^2)-1+K_{\min}^2/E_{nl}^Z]\left[\frac{df_{nl}^S}{d\epsilon}(\epsilon,0,E_{nl}^Z,Z,z)\right.$$
$$\left.-\frac{df_{nl}^S}{d\epsilon}(\epsilon,0,E_{nl}^Z,Z',0)\right]. \quad (9)$$

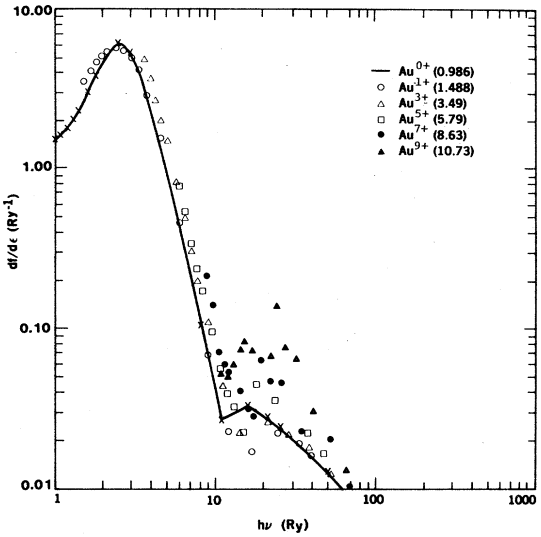

FIG. 12. The calculated $5d$ optical oscillator strength for neutral gold (solid line) and gold ions (points) normalized to ten $5d$ electrons, as a function of $h\nu=\epsilon+E_{5d}$. The photoionization thresholds are also listed.

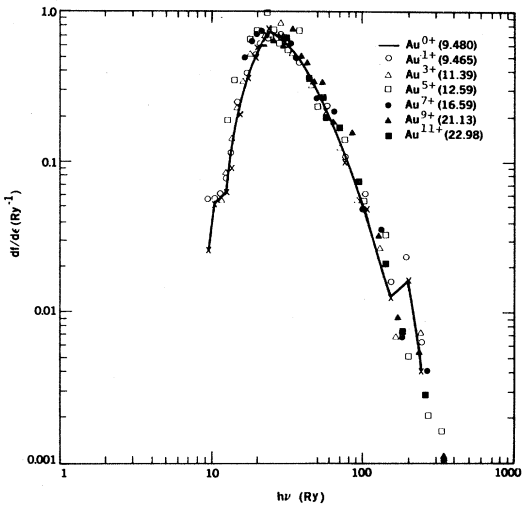

FIG. 13. The calculated $4f$ optical oscillator strength for neutral gold (solid lines) and gold ions (points) as a function of $h\nu=\epsilon+E_{4f}$. The photoionization thresholds are also listed.

Again the correction involves both ion and pseudoatom GOS and is not very useful. However, it has been shown computationally in a variety of cases[10–12] that the photoionization cross sections have the property that

$$\sigma_{nl}^{n+}(\epsilon+E_{nl}^{Z})\approx\Theta(\epsilon)\sigma_{nl}^{0}(\epsilon+E_{nl}^{Z})\,, \tag{10}$$

i.e., for the same number of electrons per shell the ion photoionization cross section approximately sits on the neutral-atom cross section when plotted as a function of photon energy. This is scaling of the photoionization cross section. To illustrate the approximate nature of the scaling, Figs. 12 and 13 show $df/d\epsilon$ at $K^2=0$ for the $5d$ (adjusted to ten electrons) and the $4f$ subshells. The results in Figs. 12 and 13 are consistent with the discussion in Ref. 13. The photoionization cross section is given by $\sigma=8\times10^{-18}df/d\epsilon$ (cm^2): The solid lines are the neutral-atom calculations and the points are optical oscillator strengths for the ions plotted as a function of $h\nu=\epsilon+E_{nl}$. The agreement is good when the cross section is large. The $5d$ cross section shows a large scatter for $10\leq h\nu\leq20$ Ry due to the sensitivity of the calculations near a zero in the $5d$-ϵf component of the cross section, i.e., where the cross section is quite small, and not contributing significantly to the stopping-power correction.

Using

$$\sigma^{n+}(\epsilon+E_{nl}^{Z})=K\frac{df_{nl}^{S}}{d\epsilon}(\epsilon,0,E_{nl}^{Z},Z,z)\,, \tag{11a}$$

$$\sigma^{0}(\epsilon'+E_{nl}^{0})=K\frac{df_{nl}^{S}}{d\epsilon}(\epsilon',0,E_{nl}^{0},Z,0)\,, \tag{11b}$$

and

$$\sigma^{n+}(\epsilon+E_{nl}^{Z})=\sigma^{0}(\epsilon+E_{nl}^{Z})\,, \tag{11c}$$

where $K=8\times10^{-18}$ cm^2, one determines $\epsilon'=\epsilon+E_{nl}^{Z}-E_{nl}^{0}$ and

$$\frac{df_{nl}^{S}}{d\epsilon}(\epsilon,0,E_{nl}^{Z},Z,z)=\frac{df_{nl}^{S}}{d\epsilon}(\epsilon+E_{nl}^{Z}-E_{nl}^{0},0,E_{nl}^{0},Z,0)\,. \tag{12}$$

Then

$$S(E,E_{nl}^{Z},Z,z)=S(E,E_{nl}^{Z},Z',0)+\frac{4\pi a_0^2}{(m_eE/m)}\int_0^{\epsilon_1}\frac{d\epsilon}{(\epsilon+E_{nl}^{Z})^{q}}\left[\frac{df_{nl}^{S}}{d\epsilon}(\epsilon+E_{nl}^{Z}-E_{nl}^{0},0,E_{nl}^{0},Z,0)-\frac{df_{nl}^{S}}{d\epsilon}(\epsilon,0E_{nl}^{Z},Z',0)\right]\times[\ln(E_{nl}^{Z}/K_{\min}^{2})-1+K_{\min}^{2}/E_{nl}^{Z}] \tag{13}$$

with

$$\epsilon_1=\left[\frac{4m_eE}{m}E_{nl}^Z\right]^{1/2}-\left[1+\frac{m_e}{m}\right]E_{nl}^Z ,$$

$$K_{\min}^2=\frac{m}{m_e}[\sqrt{E}-(E-\epsilon-E_{nl}^Z)^{1/2}]^2 .$$

This is the desired result with a correction in terms of an integral of optical oscillator strengths of the neutral atom and the neutral pseudoatom. Since pseudoatoms are nonexistent, one has to use an atom or an average of atoms with subshell ionization energy close to that of the ion subshell. For $Z\leq 54$, a complete tabulation of subshell cross sections extending down to $\epsilon=0$ is available.[14]

For Au^{3+} and Au^{9+}, the correction to the stopping power was calculated via Eq. (13). The results are shown as dashed lines in Figs. 7 and 8, with a comparison of ion and pseudoatom parameters in Table III. For Au^{3+}, the correction was negligible for the $5s$ and $5p$ subshells, but led to a small increase in the $4f$ subshell stopping power and a large decrease in the $5d$ subshell stopping power. The decrease in the $5d$ stopping power was about half the difference between scaled and explicitly calculated results. Some of the residual discrepancy arises from the use of a pseudoatom ($Z=86$) with $E_{5d}^Z=4.16$ Ry, compared to the ionic value $E_{5d}^Z=3.49$ Ry.

For Au^{9+} the optical-oscillator-strength correction had no effect on the $5p$ subshell ionization stopping power, and slightly lowered the $5s$ and $5d$ stopping power, bringing the latter values into excellent agreement with the stopping-power values calculated explicitly. Because I did not have a pseudoatom with E_{4f} near that of Au^{9+}, i.e., no calculations at $Z=87$, the $4f$ optical-oscillator-strength correction was calculated using pseudoatoms with $Z=86$ and 88, and the corrections averaged.

The scaling laws for ionization are obtained from neutral-atom calculations using a potential dropping off as $(-1/r)$ at large distances. In applying the scaling laws to ions, the difference between neutral-atom $(-1/r)$ and ion $(-z/r)$ potentials at large distances is neglected. The optical-oscillator-strength correction attempts to account for the differences in potentials, since the optical oscillator strength is particularly sensitive to the potential at large distances. For the $4f$ subshell in neutral atoms, there is a delayed maximum in the $4f$ photoionization cross section due to the angular momentum repulsion seen by continuum g electrons.[15,16] As the ion is stripped, the long-range $(-z/r)$ potential reduces the effect of the angular-momentum barrier and continuum g orbitals penetrate the atom more rapidly with increasing energy, raising the photoionization cross section near threshold. This accounts for the positive correction to the $4f$ subshell ionization stopping power. In neutral systems for $78\leq Z\leq 86$, the $5d$ photoionization cross section is large near threshold, even displaying a resonancelike structure in a one-electron calculation,[9] due to a large $5d$-ϵf matrix element. With increasing ionization the continuum f orbitals penetrate more rapidly with energy and the ionization cross section resembles the high-energy portion of the neutral-atom photoionization cross section, i.e., falls rapidly with degree of ionization as shown in Fig. 12. This accounts for the negative correction to the $5d$ subshell ionization stopping power.

Even with the optical-oscillator-strength correction, there remain significant differences between the scaled stopping powers and those calculated explicitly, e.g., the $5p$ subshell in Au^{3+} and Au^{9+} and the $5d$ subshell in Au^{9+}. An examination of the GOS in Figs. 8–10 shows that at $\epsilon/E_{nl}=25$, for $K^2/E_{nl}\leq 1$, the ion GOS is lower than the atomic GOS, even when the subshell ionization energies are the same. Since this occurs at large ϵ/E_{nl} values

TABLE III. Ion and pseudoatom subshell ionization energies used in correcting the scaled subshell stopping powers.

	Ion		Pseudoatom	
Au^{n+}; n	nl	E_{nl} (Ry)	E_{nl} (Ry)	Z(pseudoatom)
3	$4f$	11.39	11.87	82
3	$5s$	9.46	9.74	84
3	$5p$	7.20	7.16	84
3	$5d$	3.49	4.16	86
9	$4f$	21.13	16.60,25.15	86, 88
9	$5s$	17.92	17.32	90
9	$5p$	15.46	15.62	90
9	$5d$	10.73	10.94	102

where the continuum orbital significantly overlaps the bound orbital, this effect must reflect a large-scale distortion of the ion-bound orbital relative to the atom-bound orbital. In Fig. 14 a comparison is made of the $5p$ orbital for Au^{3+} with $E_{5p}=7.20$ Ry (dashed line) and the $5p$ orbital at $Z=84$ with $E_{nl}=7.16$ Ry (solid line). As Fig. 14 shows, the ion orbital is more extended. To show that this is not an artifact of the model potential, the Herman-Skillman[6] orbital values for Au^{3+} ($E_{nl}=7.21$ Ry) are shown as solid circles, and are in excellent agreement with the model orbital. As mentioned in Sec. II for gold ions, the model potential eigenvalues are in excellent agreement with the values of Herman and Skillman.[6] For the neutral atoms agreement of the eigenvalues was not as good. The $5p$ eigenvalue of Herman and Skillman at $Z=84$ is $E_{5p}=7.95$ Ry while at $Z=83$, $E_{5p}=7.20$ Ry. Thus in Fig. 14 the model orbital at $Z=84$ with $E_{5p}=7.16$ Ry (solid curve) is compared with the Herman-Skillman orbital (open circles) at $Z=83$ ($E_{5p}=7.20$). Again, the agreement is excellent. Thus, the extension of the $5p$ orbital for the ion compared to the atom appears in both Herman-Skillman and model calculations.

At $\epsilon/E_{nl}=25$, one does not expect the continuum orbital, in the spatial region where it overlaps the bound orbital, to be significantly influenced by the difference between atom and ion potentials. Then, because of the extension of the ion orbital, one expects that for the ion the continuum-bound orbital overlap will achieve a given value at a lower continuum energy than in the atomic case. For the same, large, continuum energy value the ion GOS should be lower than the atom GOS. This is a feature that cannot be accounted for in the scaling model, and is a source of residual error.

V. CONCLUSIONS

The reduction in proton stopping power by at least a factor of 2 from neutral gold to 11 times ionized gold is a striking result which should affect target design in the light ion fusion program. This conclusion is based on calculations using scaled subshell ionization stopping power. Explicit calculations on ion stopping power verified that the scaling laws could be used for inner shells with $nl \leq 4d$ for the range of ions considered here. The explicit calculations showed disagreements with the scaled subshell stopping powers of as much as a factor of 2 for $nl \geq 4f$. A correction to the scaling laws was developed in terms of an integral over optical oscillator strengths. The correction is physically reasonable and improved the agreement of explicitly calculated proton stopping powers with corrected scaled values in some cases. For other cases, the correction did not affect the agreement and it was shown that a residual error in the corrected scaling hypothesis arises from the difference between ion and atom subshell orbitals even when the ionization energies are the same. This orbital difference leads to an ionic GOS that is lower than the atom GOS at high ϵ/E_{nl} even when the subshell ionization energies are equal. However, the high ϵ/E_{nl} GOS is significant for the subshell stopping power only when the contribution of the low ϵ/E_{nl} GOS is relatively small, i.e., when there is a zero or minimum in the GOS at low ϵ/E_{nl}. That is, as shown in Figs. 9 and 10, the high-energy difference appears in the $4f$ GOS but does not affect the stopping power below 10 MeV, because the low-energy region of the GOS produces a large and broad contribution to stopping power. These calculations are being extended to more highly ionized gold ions where the $4f$ subshell should play an even more important role.

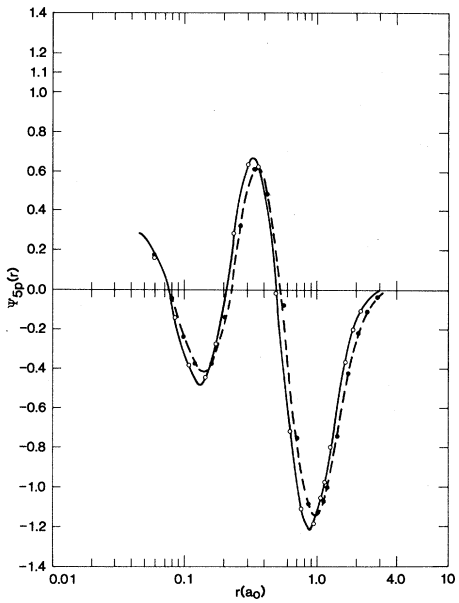

FIG. 14. The $5p$ orbital for $Z=84$ with $E_{5p}=7.16$ Ry (solid line) and Au^{3+} with $E_{5p}=7.20$ Ry, with model potentials. The solid circles are Herman-Skillman values for Au^{3+} with $E_{5p}=7.21$ Ry and the open circles are Herman-Skillman values for $Z=82$ with $E_{5p}=7.20$ Ry.

ACKNOWLEDGMENT

This work was supported by the U.S. Department of Energy.

[1]E. J. McGuire, preceding paper Phys. Rev. A 26, 1858 (1982).

[2]For C, N, and O ions see E. J. McGuire, Phys. Rev. A 25, 192 (1982); for Al ions and ions of the Na isoelectronic sequence see E. J. McGuire, Phys. Rev. A 26, 125 (1982).

[3]H. A. Bethe, Ann. Phys. (Leipzig) 5, 325 (1930); Z. Phys. 76, 293 (1932).

[4]T. A. Mehlhorn, J. Appl. Phys. 52, 6522 (1981).

[5]Y. Hahn, Phys. Rev. A 18, 1078 (1978).

[6]F. Herman and S. Skillman, *Atomic Structure Calculations* (Prentice-Hall, Englewood Cliffs, N.J., 1963).

[7]The adequacy of the straight-line approximation is discussed in E. J. McGuire, Phys. Rev. A 22, 868 (1980), and is touched on in Sec. IV.

[8]E. J. McGuire, Phys. Rev. A 16, 73 (1977).

[9]F. Combet-Farnoux, J. Phys. Paris 30, 521 (1969).

[10]W. D. Barfield, G. D. Koontz, and W. F. Huebner, J. Quant. Spect. Rad. Trans. 12, 1409 (1972).

[11]D. W. Missavage and S. T. Manson, Phys. Lett. 38A, 85 (1972).

[12]F. Combet-Farnoux and M. Lamoureux, J. Phys. B 9, 897 (1976).

[13]W. F. Huebner, M. F. Argo, and L. D. Ohlsen, J. Quant. Spect. Rad. Trans. 19, 93 (1978).

[14]E. J. McGuire, Sandia Research Report No. SC-RR-70-721 (unpublished).

[15]T. M. Zimkina, V. A. Fomichev, S. A. Gribovskii, and I. I. Zhukova, Fiz. Tverd. Tela. 9, 1447 (1967) [Sov. Phys. Solid State 9, 1128 (1967)].

[16]J. L. Dehmer, A. F. Starace, U. Fano, J. Sugar, and J. W. Cooper, Phys. Rev. Lett. 26, 1521 (1971).